Applied Thermal Engineering 212 (2022) 118472

Contents lists available at ScienceDirect

Applied Thermal Engineering

journal homepage: www.elsevier.com/locate/ate

Research paper

Molecular dynamics study of evaporation induced by locally heated argon liquid

Hirofumi Tabe, Kiryu Hiramatsu, Kazumichi Kobayashi *, Hiroyuki Fujii, Masao Watanabe, Tsuyoshi Totani

Faculty of Engineering, Hokkaido University, Kita 13, Nishi 8, Kita-ku, Sapporo, Hokkaido, 060-8628, Japan

ARTICLE INFO

Keywords:
Evaporation
Molecular dynamics
Kinetic boundary condition
Non-equilibrium

ABSTRACT

In this study, we conducted molecular dynamics simulations of the evaporation of locally heated argon liquid to construct the kinetic boundary condition (KBC) for the evaporation. The KBC denotes the boundary condition of the Boltzmann equation, and the mass, momentum, and heat fluxes through the interface can be determined by solving the Boltzmann equation with the KBC. From the results, we established a method for constructing the KBC for the evaporation of locally heated argon liquid. Furthermore, we found that the velocity distribution of the KBC immediately after liquid heating becomes anisotropic, which means that the normal and tangential temperatures composed of outgoing molecules from the liquid phase to the gas phase take different values when the liquid interface is heated momentarily. From the present study, we can elucidate the mechanism of the occurrence of net evaporation mass flux due to the locally heated liquid film, e.g., the spot heating by infrared radiation.

1. Introduction

Recently, a new drying system has attracted attention from the drying industry. This drying system uses an infrared wavelength-selective emitter [1]. For example, for drying water, this emitter irradiates infrared radiation with a peak emissivity coincident with the O–H stretching absorption band. The irradiation of the emitter induces the O–H stretching vibration of water molecules located on a liquid surface, as shown in Fig. 1. Ashihara reported that the O–H stretching vibration energy is transferred to intermolecular vibrations, such as vibrational motions [2]. Through interactions with other molecules, some molecules gain sufficient kinetic energy to overcome the potential energy binding them in place. In this sense, such molecules have a high translational temperature, referred to as excitation. As a result, these molecules fly out of the liquid surface, i.e., evaporate. Therefore, this emitter allows the system to dry at a low temperature in furnace, which prevents flammable solvents from being ignited and reduces the heat damage generated in a solute by a high temperature. The effectiveness of this device has been confirmed as shown in [1,3,4]. In Refs. [1,3], a wavelength-selective emitter with the metamaterial structure of a metal–insulator–metal, i.e., the MIM emitter, was developed to decrease large heat losses. In these studies, it was shown that the drying rate of 2-propanol when using the MIM emitter was 2.1 times higher than that achieved with a conventional wavelength-selective emitter. Moreover, in Ref. [4], it was shown that wrinkles formed in polymer films during drying by hot-air flow but not during drying by infrared irradiation, and the detailed mechanism was discussed. However, a detailed analysis of drying efficiency based on molecular theory is required because this drying system induced by infrared radiation is considered as strong non-equilibrium evaporation in which a part of the liquid phase is instantaneously heated.

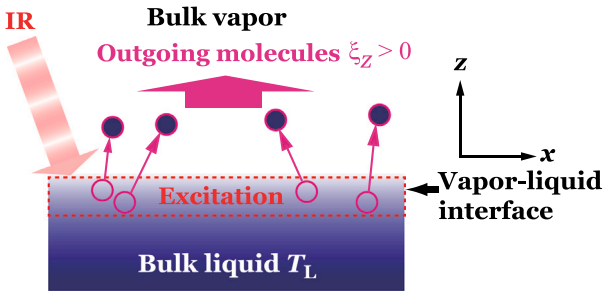

Fig. 1. Schematic of evaporation molecules induced by liquid surface excitation.

For this purpose, molecular gas dynamics analysis [5–7] is essential because the essence of evaporation and condensation phenomena is due to the non-equilibrium of molecular groups at the gas–liquid interface.

* Corresponding author.
E-mail address: kobakazu@eng.hokudai.ac.jp (K. Kobayashi).

https://doi.org/10.1016/j.applthermaleng.2022.118472
Received 9 November 2021; Received in revised form 7 March 2022; Accepted 4 April 2022
Available online 20 April 2022

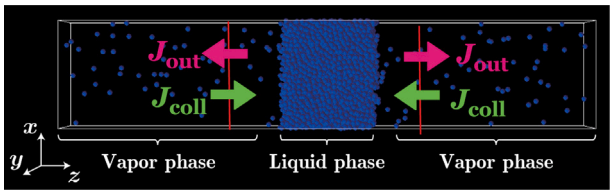

Fig. 2. Snapshot of MD simulation.

The velocity distribution function (VDF) of gas molecules is used in molecular gas dynamics analysis, where the governing equation of the VDF is the Boltzmann equation. Hence, the analysis of the Boltzmann equation is capable of treating non-equilibrium phenomena, such as evaporation and condensation. To solve the Boltzmann equation, a boundary condition called the kinetic boundary condition (KBC) is required at the vapor–liquid interface. The KBC is composed of molecules moving from the liquid phase to the vapor phase. The generalized form of the KBC [8–10] is written as

$$f_{\text{out}} = \frac{\rho_{\text{out}}}{(2\pi R)^{3/2} T_{\text{t}} \sqrt{T_{\text{n}}}} \exp\left(-\frac{\xi_x^2 + \xi_y^2}{2RT_{\text{t}}} - \frac{\xi_z^2}{2RT_{\text{n}}} \right), \text{ for } \xi_z > 0, \tag{1}$$

where f_{out} is the VDF of the outgoing molecules from the liquid phase to the vapor phase. f_{out} is the KBC of the vapor–liquid interface. $R = k/m$ is the gas constant, where k is the Boltzmann constant and m is the mass of a molecule; ξ_x, ξ_y, ξ_z are the molecular velocities of x, y, and z directions; ρ_{out} is the vapor density; and T_{n} and T_{t} are the temperatures normal and tangential to the vapor–liquid interface, respectively. ρ_{out}, T_{n}, and T_{t} are also composed of outgoing molecules with a positive ξ_z velocity, as shown in Fig. 1. For example, $T_{\text{t}} \neq T_{\text{n}} = T_0$ has been observed in a strong condensation case [8,11], where T_0 is the temperature of the bulk liquid. In previous studies, $T_{\text{t}} = T_{\text{n}} = T_0$ holds in a steady evaporation [10,12–16]. However, whether such a relationship holds in evaporation caused by a local temperature increase is unknown.

In this study, we conduct molecular dynamics (MD) simulations of the evaporation process owing to the instantaneous increase in the liquid surface temperature to modify the infrared irradiation. First, argon was targeted because it is monatomic and therefore easy to treat in MD simulations. MD is a useful tool for investigating evaporation and condensation phenomena, and various insights have been obtained from equilibrium and non-equilibrium MD calculations for single-component [17–21] and multi-component [22–25] systems using this method. However, no studies have investigated the details of molecular groups in evaporation phenomena caused by instantaneous heating at the gas–liquid interface. Therefore, our main objective is to construct the KBC for the evaporation of locally heated argon liquid using MD simulations; that is, we must identify three values: (i) the tangential temperature at the interface T_{t}, (ii) the normal temperature at the interface T_{n}, and (iii) the vapor density of outgoing molecules ρ_{out} immediately after excitation. In this study, we also propose a method for determining the KBC for the evaporation of locally heated argon liquid using MD simulations.

2. Molecular dynamics simulation

2.1. Equilibrium simulation

In this section, we describe a method for equilibrium MD simulations for argon. A system of 6000 argon molecules was considered in a simulation cell with dimensions $L_x \times L_y \times L_z$ at a temperature $T_0 = 85\,\text{K}$, where $L_x = 7.0\,\text{nm}$, $L_y = 7.0\,\text{nm}$, and $L_z = 35\,\text{nm}$ (see Fig. 2). We chose this temperature because it is close to the triple point temperature. Several studies on KBC have also been conducted using this temperature, e.g., see Refs. [8,12–14]. A vapor–liquid equilibrium was realized between the triple point (83.8 K) and the critical point (150.7 K) [12]. The liquid phase was formed at the center of the z-direction. Periodic boundary conditions were applied in all three directions of the simulation cell. As an intermolecular pair potential for argon, we employed the 12-6 Lennard-Jones potential:

$$\phi(r) = 4\epsilon \left[\left(\frac{\sigma}{r} \right)^{12} - \left(\frac{\sigma}{r} \right)^{6} \right], \tag{2}$$

where r is the distance between two interacting particles, the particle diameter σ is 3.405 Å, and the potential depth ϵ/k is 119.8 K (k is the Boltzmann constant). In general, because intermolecular interactions become weaker as the distance between two molecules increases, the cut-off radius was set as $r_c = 1.5$ nm (4.4σ) because it has been shown that $r_c > 4.0\sigma$ leads to simulation results similar to those achieved when $r_c = \infty$ [26–28]. Equations of motion were solved by using the leap–frog method.

Newton's equations of motion for the 6000 molecules in the system were integrated using the leap–frog method with a time step of 5 fs. We performed the equilibrium simulation for 200 ns and sampled the configuration of molecules (the positions and the molecular velocities of each molecule) at each time step. This yielded the number of samples $N_s = 40,000,000$.

In MD simulations, an averaged density can be calculated as

$$\rho = \frac{1}{N_{\text{s}} \Delta V} \sum_{N_{\text{s}}} \sum_{i \in \Delta V} m^i, \tag{3}$$

where ΔV is a volume element in the physical space and m^i is the mass of the ith molecule ($m^i = m$ in this study). $\sum_{i \in \Delta V}$ is the summation of the masses of the molecules contained in ΔV.

The mass flux J was also calculated by counting the number of molecules passing through per unit area per unit time [13,29]. These values are defined as follows:

$$J = \frac{mN}{S \Delta t}, \tag{4}$$

where N is the number of sample molecules for each trajectory stated above, and S is the cross-section of the system. The equilibrium simulation produced the following averaged quantities: bulk vapor density ρ_v; bulk liquid density ρ_ℓ; mass flux of outgoing molecules from the liquid phase to the vapor phase J_{out}, which is composed of the molecules of f_{out}; and mass flux of molecules colliding onto the liquid phase J_{coll}, which is composed of the molecules of f_{coll}, where f_{coll} is the VDF with a negative velocity $\xi_z < 0$ at the right-hand side vapor–liquid interface in Fig. 2 (For the left-hand side interface, J_{out} is composed of the molecules having negative ξ_z, and J_{coll} is composed of the molecules having positive ξ_z). The net mass flux $\dot{m}$ can be defined as follows:

$$\dot{m} = J_{\text{out}} - J_{\text{coll}}. \tag{5}$$

In the case of an equilibrium, $J_{\text{out}} = J_{\text{coll}}$, which leads to $\dot{m} = 0$. In the case of net evaporation, $\dot{m}$ takes positive values because $J_{\text{out}} > J_{\text{coll}}$.

The spatial density distribution near the transition layer is shown in Fig. 3. In order to determine the approximate location of the center of the transition layer and its thickness, which is known to be asymmetric in practice [30,31], the following equation was used to estimate the thickness [29].

$$\rho(z) = \frac{\rho_v + \rho_\ell}{2} + \frac{\rho_v - \rho_\ell}{2} \tanh\left(\frac{z - Z_m}{0.455\delta} \right), \tag{6}$$

where Z_m is the center of the transition layer and δ is the 10–90 thickness. In an equilibrium state at temperature T_0, the vapor density ρ_v becomes ρ_v^*, where ρ_v^* denotes the saturated vapor density at T_0, and ρ_ℓ becomes ρ_ℓ^*, where ρ_ℓ^* denotes the liquid density in the equilibrium state at T_0. The values of Z_m and δ were determined by the nonlinear least-squares method using the density distribution. The value of saturated vapor density is 4.86 kg/m^3 and the value of liquid density is 1388.44 kg/m^3 in this simulations. We confirmed that these values are in agreement with those of previous studies (i.e., Refs. [8,29]). A

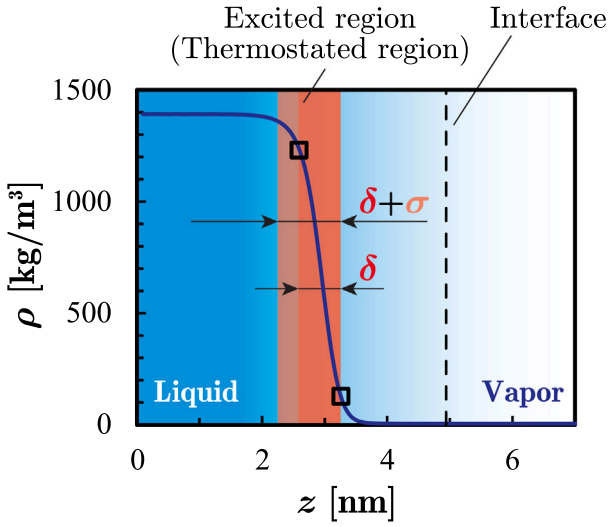

Fig. 3. Schematic of excited region at liquid surface, (a) $\delta+\sigma$ and (b) δ. The density profile is represented by Eq. (6). The squares indicate the edges of the transition layer. The dotted line indicates the interface position for imposing the KBC.

previous study demonstrated that for vapor–liquid equilibrium systems of Ar molecules, vapor can be treated as an ideal gas at temperatures below 100 K [8]. Therefore, the vapor in the initial state can be considered as an ideal gas in this study.

The position to impose the KBC is defined as $z = Z_m + 3\delta$. At this position, the influence of the intermolecular potential force composed of liquid molecules becomes sufficiently small to be ignored. This is why Eq. (1) does not include the effect of the liquid potential. The validity of this position has been discussed in our previous studies [13,29,32].

2.2. Excitation (thermostatting)

This section describes how to excite the liquid surface to simulate infrared irradiation drying. Essentially, there are two factors that lead to more evaporation: (i) higher excitation temperature, and (ii) a thicker excited region. Now, we explain the excited region and the method for exciting the liquid surface. Because it is difficult to know the detailed information of excitation experimentally, we investigate the evaporation process by changing the excited region and excitation temperature based on MD simulations.

In this study, we used two types of excited regions (see Fig. 3). Here, we consider that many molecules in the first layer at the liquid surface are excited, and we performed MD simulations for the following two cases. The difference is the thickness of the excited region. One is the 10–90 thickness δ (8.85 Å) + the argon diameter σ (3.405 Å). The other is the 10–90 thickness δ. The vapor-side edge of the excited region for each case coincides with the edge of the transition layer, as shown in Fig. 3.

To excite the region, we increased the molecular velocities of the argon molecules contained in these regions using velocity scaling [33]. In velocity scaling, the j component of the molecular velocity of the i th molecule ξ_j^i is transformed to $\xi_j^{i\prime}$ through the following rule:

$$\xi_j^{i\prime} = \sqrt{\frac{T_{\mathrm{exc}}}{T}}\,\xi_j^i \qquad (j = x, y, z), \tag{7}$$

where T_{exc} is the target temperature and T is the temperature immediately before excitation. This corresponds to thermostatting the molecules in a certain region, which we call excitation in this study. Thus, we can instantly increase the temperature of the excited region to the target temperature T_{exc}. Hereafter, we refer to the target temperature T_{exc} as the excitation temperature.

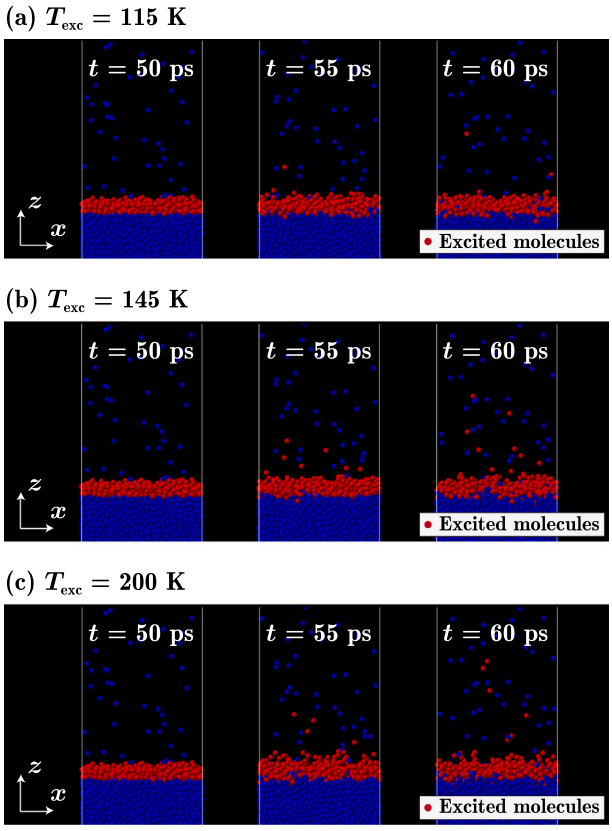

Fig. 4. Snapshots of MD simulation at the moment of excitation when T_{exc} = 115 K, 145 K, and 200 K in the case of $\delta+\sigma$. Red molecules indicate excited molecules. Excitation is started at t = 50 ps.

Here, we chose several excitation temperatures: T_{exc} = 95, 100, 105, 115, 130, 145, and 200 K. An excitation temperature of T_{exc} = 200 K is still high, considering that the critical temperature of argon is 150.7 K.

3. Results

3.1. Net evaporation mass flux $\dot{m}$

We present the results of this study. MD simulations for excitation evaporation using 1000 initial conditions obtained by equilibrium simulations were conducted, and the averages of the 1000 MD simulations are reflected in the following results. We focus on the results of the excitation temperature T_{exc} = 115 K, 145 K, and 200 K. Snapshots of the MD simulation at the time of excitation in the T_{exc} = 115 K, 145 K, and 200 K cases are shown in Fig. 4. The red molecules denote the excitation molecules in the case of $\delta+\sigma$. When the time is t = 50 ps, the molecules in the excited region are excited in accordance with Eq. (7). It can then be seen that the excited molecules interact with other molecules and fly toward the vapor region, i.e., evaporation occurs due to excitation.

Fig. 5 shows the temporal evolutions of J_{out} and J_{coll} for T_{exc} = 115 K, 145 K, and 200 K, respectively. The dotted line in each figure is J^*_{out} or J^*_{coll}, where J^*_{out} and J^*_{coll} are the outgoing and colliding molecular mass fluxes at the equilibrium state, respectively. We can easily obtain $J^*_{\mathrm{out}} = J^*_{\mathrm{coll}} = \rho^*_v\sqrt{RT_0/2\pi}$ from Eq. (1) in the equilibrium state ($\rho_{\mathrm{out}} = \rho^*_v$ and $T_{\mathrm{n}} = T_{\mathrm{t}} = T_0$). From Figs. 5(a), (b) and (c), we can observe that J_{out} becomes larger than J^*_{out}, which leads to the evaporation of liquid molecules due to excitation for the cases of $\delta+\sigma$ and δ. As the excited region becomes thicker, the evaporation mass flux increases.

The peak times of J_{out} are shifted to the right from t = 50 ps because excited molecules take time to reach the interface as shown

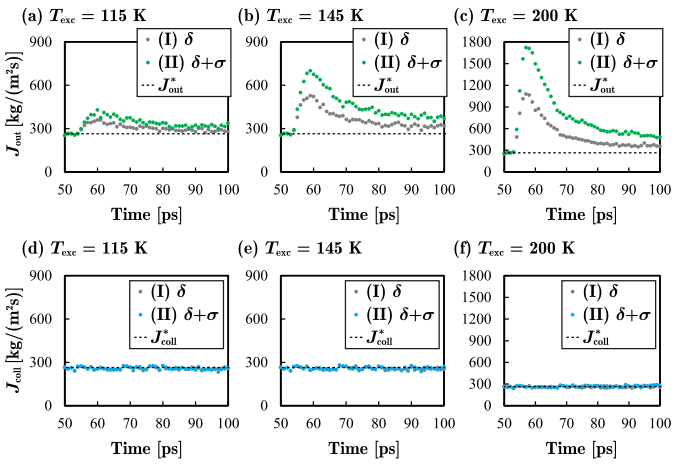

Fig. 5. Temporal evolutions of J_{out} and J_{coll}. (a) and (d); T_{exc} = 115 K, (b) and (e); T_{exc} = 145 K, (c) and (f); T_{exc} = 200 K.

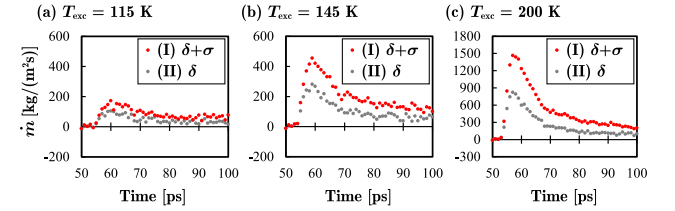

Fig. 6. Temporal evolutions of net evaporation mass flux $\dot{m}$. (a) T_{exc} = 115 K, (b) T_{exc} = 145 K, and (c) T_{exc} = 200 K.

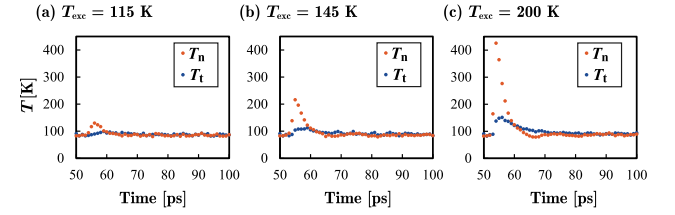

Fig. 7. Temporal evolutions of tangential temperature T_t and normal temperature T_n. The blue circles represent T_t and the orange circles represent T_n. (a) T_{exc} = 115 K, (b) T_{exc} = 145 K, and (c) T_{exc} = 200 K.

in Figs. 5(a), (b), and (c). We can estimate the time for molecules to travel from the center of the excited region to the interface, Δt_f, by using the most probable speed of vapor molecules, $v_p = \sqrt{2RT_{exc}}$. When the excited region is δ, the times are Δt_f = 9.19 ps, Δt_f = 8.18 ps, and Δt_f = 6.97 ps for 115 K, 145 K, and 200 K, respectively; when the region is $\delta + \sigma$, the times are Δt_f = 9.96 ps, Δt_f = 8.87 ps, and Δt_f = 7.55 ps. According to these results, the Δt_f values in both cases are almost the same at each peak time, as shown in Figs. 5(a), (b), and (c).

However, as shown in Figs. 5(d), (e), and (f), the values of J_{coll} are constant, $J_{coll} = J^*_{coll}$. These results indicate that the excited molecules do not interact with the molecules colliding from the vapor phase to the liquid phase, and that net evaporation occurs in the present MD simulations.

The temporal changes in the net evaporation mass flux $\dot{m}$ in the evaporation simulation for T_{exc} = 115 K, 145 K, and 200 K are plotted in Fig. 6 obtained from Eq. (5). After t = 50 ps, $\dot{m}$ increases in both cases due to excitation. The peak of $\dot{m}$ becomes higher as the value of T_{exc} increases. Evaporation continues after 100 ps, after which the system returns to equilibrium.

Although there is a difference in the amount of evaporation, we will discuss the above results of $\delta + \sigma$ in the following, as it was confirmed that there is no difference in evaporation tendency between the excited regions δ and $\delta + \sigma$.

3.2. Velocity distribution at the interface

In this section, we discuss the velocity distribution function of the outgoing molecules at the interface, namely, the kinetic boundary condition.

First, we focus on the tangential temperature T_t and the normal temperature T_n to make use of the KBC form in Eq. (1). These temperatures are obtained by the following equations:

$$\frac{1}{2}kT_t = \sum_{N_s} \frac{1}{2}m\frac{\xi_x^2 + \xi_y^2}{2N_s}, \tag{8}$$

$$\frac{1}{2}kT_n = \sum_{N_s} \frac{1}{2}m\frac{\xi_z^2}{N_s}, \tag{9}$$

where the above equations are for molecules outgoing from liquid to vapor, e.g., in Fig. 1, the equation consists of molecules with positive velocities ξ_z. Fig. 7 shows the temporal evolutions of T_t and T_n for each excitation temperature and the excited region $\delta+\sigma$. In the case of T_{exc} = 115 K, T_n is greater than T_0 for 52 ps $\leq t \leq$ 60 ps, whereas T_t remains approximately 85 K. In contrast, in the cases of T_{exc} = 145 K and 200 K, T_n has a higher peak and T_t has a small peak after a short delay. These temperature differences lead to the anisotropy of the VDF at the vapor–liquid interface.

Here, we take the time average of T_t and T_n for 52 ps $\leq t \leq$ 60 ps to treat the pulsate changes in the temperatures. Using these temperatures, we construct the KBC, given by Eq. (1), for each excitation temperature.

Fig. 8 shows the velocity distribution function of $\hat{f}_{out} = \hat{f}_x\hat{f}_y\hat{f}_z$, where $\hat{}$ denotes the normalization, and $\hat{f}_j$ ($j = x, y, z$) denotes the normalized VDF for the j-component, where $\hat{f}_x = \hat{f}_y$ in this study. We plot the time-averaged velocity distributions for 52 ps $\leq t \leq$ 60 ps of the outgoing molecules at the interface, which were obtained by the MD simulations. The time-averaged velocity distributions for Figs. 8(a) and (d) T_{exc} = 115 K, Figs. 8(b) and (e) T_{exc} = 145 K, and Figs. 8(c) and (f) T_{exc} = 200 K are made up of 8920, 13,234, and 30,706 molecules, respectively. Here, because the KBCs and time-averaged velocity distributions are normalized, their velocity distribution functions indicate the probability of existence of the molecule. The abscissa $\zeta_j = \xi_j/\sqrt{2RT_0}$ is the j component of the normalized molecular velocity, where T_0 = 85 K.

As shown in Fig. 8(a), the velocity distribution for the tangential direction $\hat{f}_x$ agrees with a solid curve, the normalized Maxwellian $\sqrt{T_0/(T_t\pi)}\exp(-\zeta_x^2 T_0/T_t)$ with T_t = 89.6 K for T_{exc} = 115 K. For the cases of T_{exc} = 145 K and 200 K in Figs. 8(b) and (c), $\hat{f}_x$ also agrees with a normalized Maxwellian with T_t = 100.3 K and 126.5 K. We can say that the outgoing molecules have a velocity distribution in the tangential direction at T_0 = 85 K in the case of low excitation temperature because T_t is nearly equal to T_0.

From Fig. 8(d), the velocity distribution function for the normal direction $\hat{f}_z$ can be almost fitted by the normalized Maxwellian $2T_0/T_n\zeta_z\exp(-\zeta_z^2 T_0/T_n)$ with T_n = 105.3 K for T_{exc} = 115 K. The value of T_n = 105.3 K is much larger than the tangential temperature T_t = 89.6 K (see Fig. 8(a)). In the cases of T_{exc} = 145 K and 200 K (Figs. 8(e) and (f)), $\hat{f}_z$ is slightly different from the normalized Maxwellian with T_n = 141.1 K or 217.5 K. The values of T_n are also larger than the tangential temperatures T_t = 100.3 K and 126.5 K. We confirm that the normal temperature takes the approximate value of the excitation temperature. For the VDF in the normal direction, an almost Maxwell distribution with an excitation temperature is observed in the MD simulation of a heated ultra-thin liquid layer [34]. Our results agree with the previous MD simulation except for the extremely high excitation temperature having the deviation from the Maxwellian, as shown in Fig. 8(f).

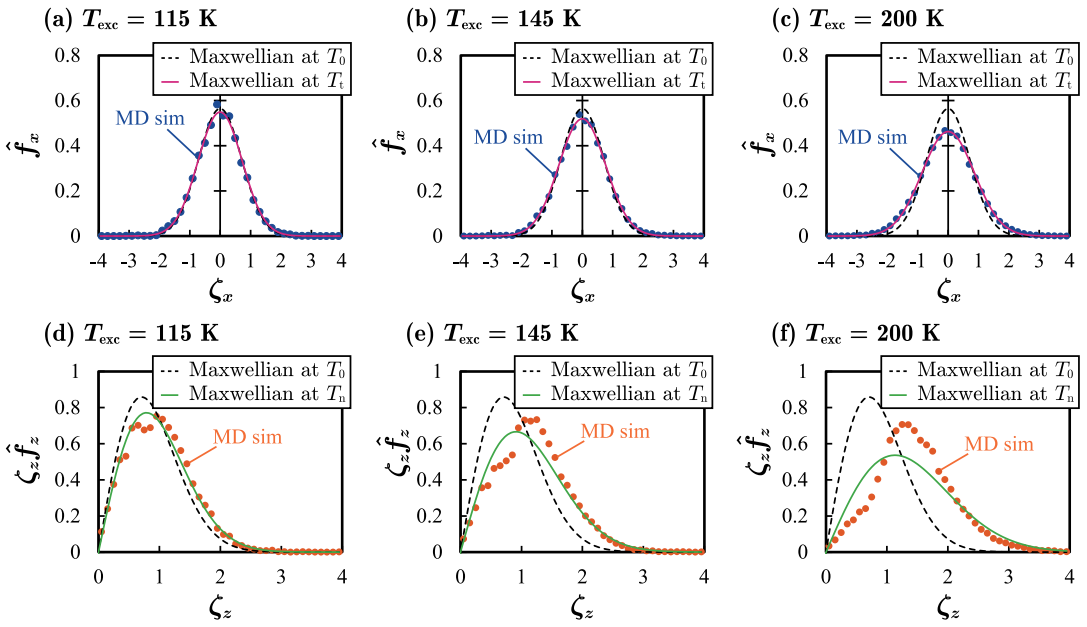

Fig. 8. Normalized velocity distribution at the interface. (a) $\hat{f}_x$, T_{exc} = 115 K (T_t = 89.6 K, T_0 = 85 K); (b) $\hat{f}_x$, T_{exc} = 145 K (T_t = 100.3 K, T_0 = 85 K); (c) $\hat{f}_x$, T_{exc} = 200 K (T_t = 126.5 K, T_0 = 85 K); (d) $\hat{f}_z$, T_{exc} = 115 K (T_n = 105.3 K, T_0 = 85 K); (e) $\hat{f}_z$, T_{exc} = 145 K (T_n = 141.1 K, T_0 = 85 K); (f) $\hat{f}_z$, T_{exc} = 200 K (T_n = 217.5 K, T_0 = 85 K).

The anisotropy of VDF at the KBC is thought that by increasing the temperature of the liquid, the molecules with fast positive velocity in the z-direction, i.e., the normal direction to the interface from the liquid phase to the vapor phase, will evaporate and pass through the interface position near the density transition layer where the VDF is measured. In previous studies, it was shown that the molecules having fast positive velocity in the normal direction can evaporate, that is, the evaporation probability increases with the increase in the normal direction velocity [29,35,36]. On the other hand, the molecules with slow positive velocities in the z-direction are less likely to evaporate and will take longer to pass through the interface where the VDF is measured. In addition, the molecules with slow positive velocities have more time to interfere with the liquid phase, so they tend to lose the effect of warming the liquid film. This effect would result in a smaller number of molecules with low z-direction velocity being measured, compared to molecules with relatively high z-direction velocity in the VDF. The detailed mechanism of the deviation will be a focus of our future work.

3.3. Excitation temperature dependence of T_t, T_n, and ρ_{out}

Fig. 9 shows T_t, T_n, and ρ_{out} as functions of T_{exc}. These values are the time-averaged values for 52 ps $\le t \le$ 60 ps, which show the values immediately after the excitation of the liquid surface. We can obtain the vapor density of outgoing molecules ρ_{out}. f_{out}, ρ_{out}, and J_{out} have the following relation:

$$J_{out} = \int_{-\infty}^{\infty}\int_{-\infty}^{\infty}\int_{0}^{\infty} \xi_z f_{out} d\xi_z d\xi_x d\xi_y = \rho_{out}\sqrt{\frac{RT_n}{2\pi}}. \quad (10)$$

From the above equation, we can obtain the following equation for ρ_{out} and calculate its value using J_{out} and T_n:

$$\rho_{out} = \frac{J_{out}}{\sqrt{RT_n/2\pi}}. \quad (11)$$

Note that the error in this procedure increases as the excitation temperature increases, because the deviation from the Maxwellian at T_n becomes larger when the excitation temperature is higher. Fig. 9(a) shows T_t and T_n. The solid line denotes $T_n = T_{exc}$, and the dotted line in Fig. 9(a) denotes T_0 = 85 K. As shown in Fig. 9(a), T_n increases with T_{exc}, and the value T_n is almost the same as T_{exc}, which leads to $T_n \approx T_{exc}$. In contrast, for T_t, the value is slightly higher than the initial value T_0 in the case of high excitation temperature. However, for low excitation temperature (approximately T_{exc} < 100 K), $T_t \approx T_0$.

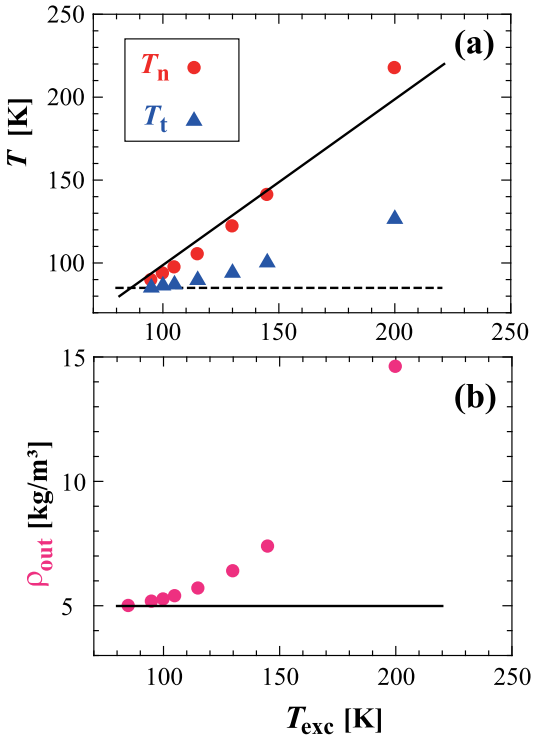

Fig. 9. (a) T_n and T_t composed of evaporating molecules as a function of T_{exc}; (b) ρ_{out} composed of evaporation molecules as a function of T_{exc}.

Fig. 9(b) shows ρ_{out}. The solid line denotes the saturated vapor density at T_0. As shown in the figure, the value of ρ_{out} increases with an increase in T_{exc}. However, when T_{exc} takes a small value, we can assume that $\rho_{out} \approx \rho_v^*(T_0)$.

We now obtain all three values: (i) the tangential temperature at the interface T_t, (ii) the normal temperature at the interface T_n, and (iii) the vapor density of outgoing molecules ρ_{out}. In addition, we confirm that the outgoing molecules almost leave the interface with the KBC form of Eq. (1). Therefore, KBC can be constructed using Eq. (1) with these values. From the above discussion, we can rewrite the KBC as

$$f_{out} = \frac{\rho_{out}}{(2\pi R)^{3/2} T_t \sqrt{T_{exc}}} \exp\left(-\frac{\xi_x^2 + \xi_y^2}{2RT_t} - \frac{\xi_z^2}{2RT_{exc}} \right), \tag{12}$$

where $T_n = T_{exc}$. ρ_{out} and T_t are functions of T_{exc}, as shown in Fig. 9. Moreover, we can obtain the colliding mass flux as $J_{coll} = \rho_v^*(T_0)\sqrt{RT_{exc}/2\pi}$ as shown in Fig. 5. Using J_{out} and J_{coll}, the following mass flux can be obtained immediately after excitation:

$$\dot{m} = \rho_{out} \sqrt{\frac{RT_0}{2\pi}} \left(\sqrt{\frac{T_{exc}}{T_0}} - 1 \right). \tag{13}$$

From the above equation, we can estimate the net mass flux $\dot{m}$ immediately after excitation of the liquid surface in the case of low excitation temperature.

4. Conclusion

In this study, we conducted MD simulations of the evaporation of locally heated argon liquid to construct the kinetic boundary conditions for the evaporation. We also proposed a method for constructing the KBC for the evaporation of locally heated argon liquid. From the results, we found that the velocity distribution of the KBC becomes anisotropic, which means that the tangential and normal temperatures composed of outgoing molecules from the liquid phase to the gas phase take different values when the liquid interface is heated momentarily. The normal temperature T_n agrees with the excitation temperature T_{exc} and the tangential temperature T_t is almost the same as the initial temperature T_0 in the case in which the difference between T_{exc} and T_0 is not very large.

From this study, we were able to demonstrate the non-equilibrium nature of the evaporation phenomenon induced on the surface of a liquid with an instantaneous temperature increase by studying the behavior of the molecules. As a result, a boundary condition for the Boltzmann equation for this problem was proposed. This is a novelty in this research. By using the proposed boundary condition, the evaporation rate of the instantaneously excited interfaces can be obtained through the Boltzmann equation analysis. In future work, we will conduct the evaporation with polyatomic molecules [37], e.g., water molecules, to simulate the actual drying phenomenon. In addition, the evaporation of a multi-component system [32,38–41] is an important topic. It has been found that the composition of molecules at the liquid or gas–liquid interface is important for multi-component evaporation [42]. Examining the composition of such interfaces and the detailed behavior of evaporated molecules are two of our future research themes.

Declaration of competing interest

The authors declare that they have no known competing financial interests or personal relationships that could have appeared to influence the work reported in this paper.

Acknowledgments

This work was supported by JSPS, Japan KAKENHI Grant Number JP 19H02074 to T.T., 20K04277 to K.K., and f3 Engineering Education and Research Center, Faculty of Engineering, Hokkaido University to K.K., and JST, PRESTO, Japan Grant Number JPMJPR21O3, Japan to K.K.

References

[1] T. Totani, A. Sakurai, T.D. Dao, T. Nagao, Y. Kondo, Application of the wavelength selective emitter with the metamaterial of a metal-insulator-metal to an infrared ray drying furnace, in: International Heat Transfer Conference Digital Library, Begel House Inc. 2018.
[2] S. Ashihara, Time-resolved observation of molecular dynamics in liquid water by mid-infrared nonlinear spectroscopy(in Japanese), Kougaku 40 (8) (2011) 409–414.
[3] T. Totani, A. Sakurai, T. Nagao, Y. Kondo, Increase of drying rate by wavelength-selective emitter with metamaterial structures in infrared ray drying, in: Extended Abstracts of the Second Pacific Rim Thermal Engineering Conference, 2019.
[4] T. Kinnan, Y. Kondo, M. Aoki, S. Inasawa, How do drying methods affect quality of films? Drying of polymer solutions under hot-air flow or infrared heating with comparable evaporation rates, Dry. Technol. (2020) 1–12.
[5] G.A. Bird, Molecular Gas Dynamics and the Direct Simulation of Gas Flows, Clarendon press Oxford, 1994.
[6] C. Cercignani, Rarefied Gas Dynamics: From Basic Concepts to Actual Calculations, Cambridge University Press, 2000.
[7] Y. Sone, Molecular Gas Dynamics, Birkhäuser, 2007.
[8] T. Ishiyama, T. Yano, S. Fujikawa, Kinetic boundary condition at a vapor-liquid interface, Phys. Rev. Lett. 95 (2005) 084504.
[9] A. Frezzotti, Boundary conditions at the vapor-liquid interface, Phys. Fluids 23 (3) (2011) 030609.
[10] M. Kon, K. Kobayashi, M. Watanabe, Method of determining kinetic boundary conditions in net evaporation/condensation, Phys. Fluids 26 (7) (2014) 072003.
[11] A. Tokunaga, T. Tsuruta, Nonequilibrium molecular dynamics study on energy accommodation coefficient on condensing liquid surface-molecular boundary conditions for heat and mass transfer, Phys. Fluids 32 (11) (2020) 112011.
[12] T. Ishiyama, T. Yano, S. Fujikawa, Molecular dynamics study of kinetic boundary condition at an interface between argon vapor and its condensed phase, Phys. Fluids 16 (8) (2004) 2899–2906.
[13] K. Kobayashi, K. Hori, M. Kon, K. Sasaki, M. Watanabe, Molecular dynamics study on evaporation and reflection of monatomic molecules to construct kinetic boundary condition in vapor-liquid equilibria, Heat Mass Trans. 52 (9) (2016) 1851–1859.
[14] M. Kon, K. Kobayashi, M. Watanabe, Liquid temperature dependence of kinetic boundary condition at vapor-liquid interface, Int. J. Heat Mass Trans. (ISSN: 0017-9310) 99 (2016) 317–326.
[15] M. Kon, K. Kobayashi, M. Watanabe, Kinetic boundary condition in vapor-liquid two-phase system during unsteady net evaporation/condensation, Eur. J. Mech. - B/Fluids (ISSN: 0997-7546) 64 (2017) 81–92, Special Issue on Non-equilibrium Gas Flows.
[16] V.V. Zhakhovsky, A.P. Kryukov, V.Y. Levashov, I.N. Shishkova, S.I. Anisimov, Mass and heat transfer between evaporation and condensation surfaces: Atomistic simulation and solution of Boltzmann kinetic equation, Proc. Natl. Acad. Sci. 116 (37) (2019) 18209–18217.
[17] C. Braga, J. Muscatello, G. Lau, E.A. Müller, G. Jackson, Nonequilibrium study of the intrinsic free-energy profile across a liquid-vapour interface, J. Chem. Phys. 144 (4) (2016) 044703.
[18] A. Lotfi, J. Vrabec, J. Fischer, Evaporation from a free liquid surface, Int. J. Heat Mass Trans. 73 (2014) 303–317.
[19] M. Heinen, J. Vrabec, Evaporation sampled by stationary molecular dynamics simulation, J. Chem. Phys. 151 (4) (2019) 044704.
[20] Z. Liang, A. Chandra, E. Bird, P. Keblinski, A molecular dynamics study of transient evaporation and condensation, Int. J. Heat Mass Trans. (ISSN: 0017-9310) 149 (2020) 119152.
[21] B. Ma, K. Guye, B. Dogruoz, D. Agonafer, Molecular dynamics simulations of thin-film evaporation: The influence of interfacial thermal resistance on a graphene-coated heated silicon substrate, Appl. Therm. Eng. (ISSN: 1359-4311) 195 (2021) 117142.
[22] V. Baidakov, S. Protsenko, Molecular-dynamics simulation of relaxation processes at liquid–gas interfaces in single-and two-component lennard-jones systems, Coll. J. 81 (5) (2019) 491–500.
[23] V.G. Baidakov, S.P. Protsenko, V.M. Bryukhanov, Relaxation processes at liquid-gas interfaces in one-and two-component lennard-jones systems: Molecular dynamics simulation, Fluid Ph. Equilib. 481 (2019) 1–14.
[24] S. Cai, Q. Li, C. Liu, L. Zhang, Evaporation of Ar/Kr mixtures on platinum surface: a molecular dynamics study, Phys. Chem. Chem. Phys. 22 (28) (2020) 16157–16164.
[25] S. Stephan, D. Schaefer, K. Langenbach, H. Hasse, Mass transfer through vapour–liquid interfaces: A molecular dynamics simulation study, Mol. Phys. 119 (3) (2021) e1810798.
[26] C. Holcomb, P. Clancy, S. Thompson, J. Zollweg, A critical study of simulations of the lennard-jones liquid-vapor interface, Fluid Ph. Equilib. 75 (1992) 185–196.
[27] A. Trokhymchuk, J. Alejandre, Computer simulations of liquid/vapor interface in lennard-jones fluids: Some questions and answers, J. Chem. Phys. 111 (18) (1999) 8510–8523.

[28] H. Yaguchi, T. Yano, S. Fujikawa, Molecular dynamics study of vapor-liquid equilibrium state of an argon nanodroplet and its vapor, J. Fluid Sci. Tech. 5 (2) (2010) 180–191.
[29] H. Tabe, K. Kobayashi, H. Fujii, M. Watanabe, Molecular dynamics study on characteristics of reflection and condensation molecules at vapor–liquid equilibrium state, PLoS One 16 (3) (2021) e0248660.
[30] B.Q. Lu, R. Evans, M. Telo da Gama, The form of the density profile at a liquid-gas interface: Dependence on the intermolecular potential, Mol. Phys. 55 (6) (1985) 1319–1338.
[31] S. Stephan, J. Liu, K. Langenbach, W.G. Chapman, H. Hasse, Vapor- liquid interface of the lennard-jones truncated and shifted fluid: Comparison of molecular simulation, density gradient theory, and density functional theory, J. Phys. Chem. C 122 (43) (2018) 24705–24715.
[32] K. Ohashi, K. Kobayashi, H. Fujii, M. Watanabe, Evaporation coefficient and condensation coefficient of vapor under high gas pressure conditions, Sci. Rep. 10 (1) (2020) 1–10.
[33] M.P. Allen, D.J. Tildesley, Computer Simulation of Liquids, Oxford, 1987.
[34] P. Yi, D. Poulikakos, J. Walther, G. Yadigaroglu, Molecular dynamics simulation of vaporization of an ultra-thin liquid argon layer on a surface, Int. J. Heat Mass Trans. (ISSN: 0017-9310) 45 (10) (2002) 2087–2100.
[35] T. Tsuruta, H. Tanaka, T. Masuoka, Condensation/evaporation coefficient and velocity distributions at liquid–vapor interface, Int. J. Heat Mass Trans. 42 (22) (1999) 4107–4116.
[36] T. Tsuruta, G. Nagayama, Molecular dynamics studies on the condensation coefficient of water, J. Phys. Chem. B 108 (5) (2004) 1736–1743.
[37] S. Busuioc, L. Gibelli, Mean-field kinetic theory approach to langmuir evaporation of polyatomic liquids, Phys. Fluids 32 (9) (2020) 093314.
[38] K. Kobayashi, K. Sasaki, M. Kon, H. Fujii, M. Watanabe, Kinetic boundary conditions for vapor–gas binary mixture, Microfluid Nanofluid 21 (3) (2017) 53.
[39] A. Frezzotti, L. Gibelli, D.A. Lockerby, J.E. Sprittles, Mean-field kinetic theory approach to evaporation of a binary liquid into vacuum, Phys. Rev. Fluids 3 (2018) 054001.
[40] K. Ohashi, K. Kobayashi, H. Fujii, M. Watanabe, Mean-field kinetic theory analysis of vapor flow between evaporating and condensing interfaces in the presence of non-condensable gas molecules, Phys. Fluids 33 (12) (2021) 122017.
[41] H. Tabe, K. Kobayashi, H. Fujii, M. Watanabe, Molecular dynamics simulation of evaporation coefficient of vapor molecules during steady net evaporation in binary mixture system, Int. J. Heat Mass Trans. 188 (2022) 122663.
[42] S. Stephan, H. Hasse, Enrichment at vapour–liquid interfaces of mixtures: establishing a link between nanoscopic and macroscopic properties, Int. Rev. Phys. Chem. 39 (3) (2020) 319–349.